Additive manufacturing of Aluminium alloys

Contents

Introduction

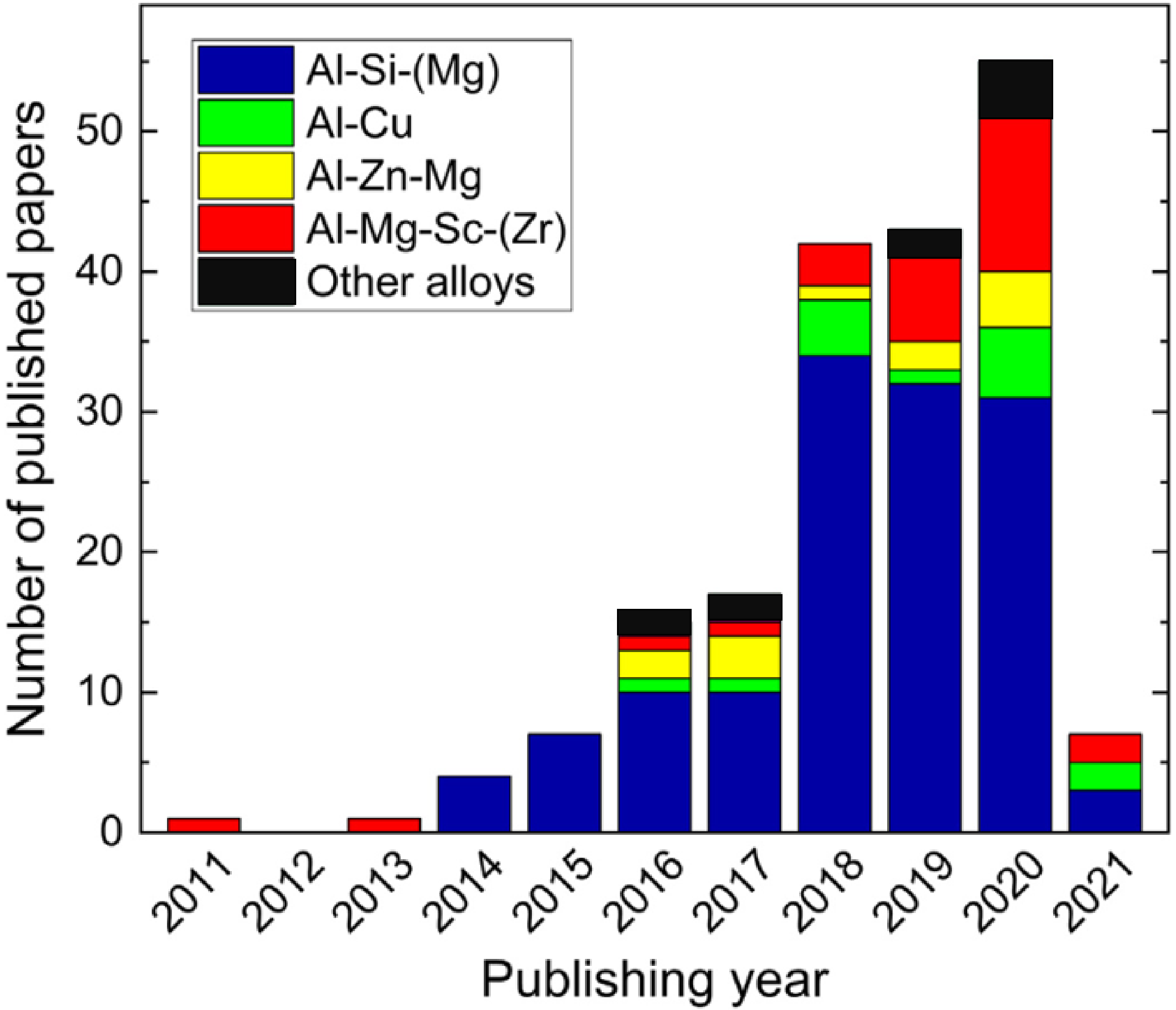

Fig. LPBFed aluminum alloy papers that have been published in recent years

Source: Fiocchi et al. 2021 [https://doi.org/10.1016/j.matdes.2021.109651]

AlSi10Mg

Table: Chemical composition (%wt.) of aluminium alloys studied in this chapter

Alloy	Al	Si	Mg	Ti	Mn	Fe	Cu	Zn	Sc	Zr	Cr
AlSi10Mg	Bal.	8.5–10.5	0.2–0.5	<0.15	-	<0.9	<0.15	<0.1	-	-	-
AlSi12	Bal.	10.5–13.5	-	<0.15	-	<0.4	-	<0.1	-	-	-
Scalmalloy	Bal.	<0.4	4–4.9	<0.15	0.3–0.8	<0.4	<0.1	<0.25	0.6–0.8	0.2–0.5	-
AlSi7Mg	Bal.	6.5–7.5	0.5–0.8	<0.2	<0.1	<0.2	<0.05	<0.1	-	-	-
AA6061	Bal.	0.4–0.8	0.8–1.2	<0.15	<0.15	<0.7	0.15–0.4	<0.25	-	-	0.04–0.35

AlSi10Mg

Fig. A section of AlSi10Mg phase diagram for 0.4 wt.% of Mg, where α denotes the Al matrix. The orange line shows the solidification order of the nominal composition of the alloy in equilibrium. The blue dashed line shows the eutectic (E) composition

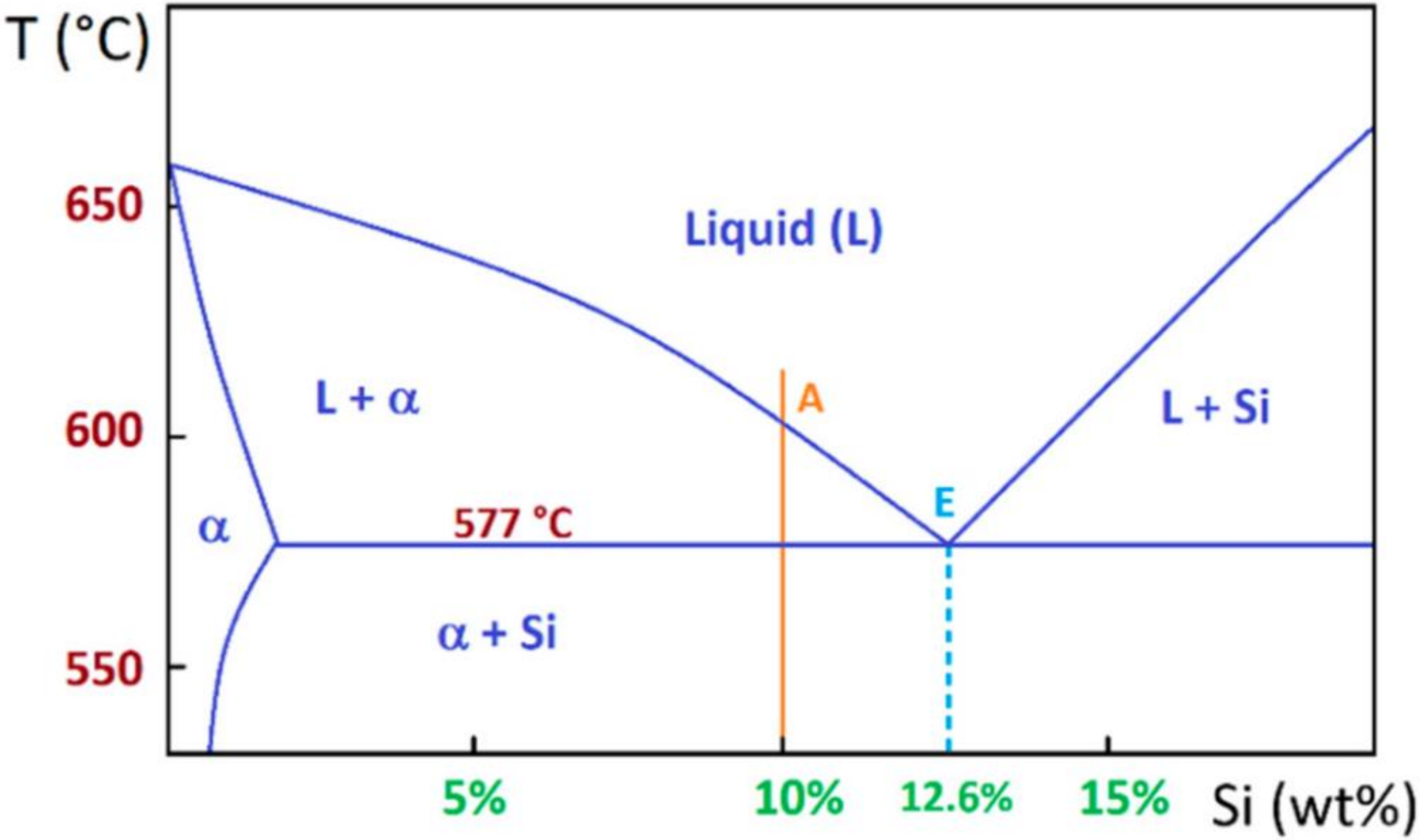

Source: Ghio et al. 2022 [https://doi.org/10.3390/ma15062047]

AlSi10Mg

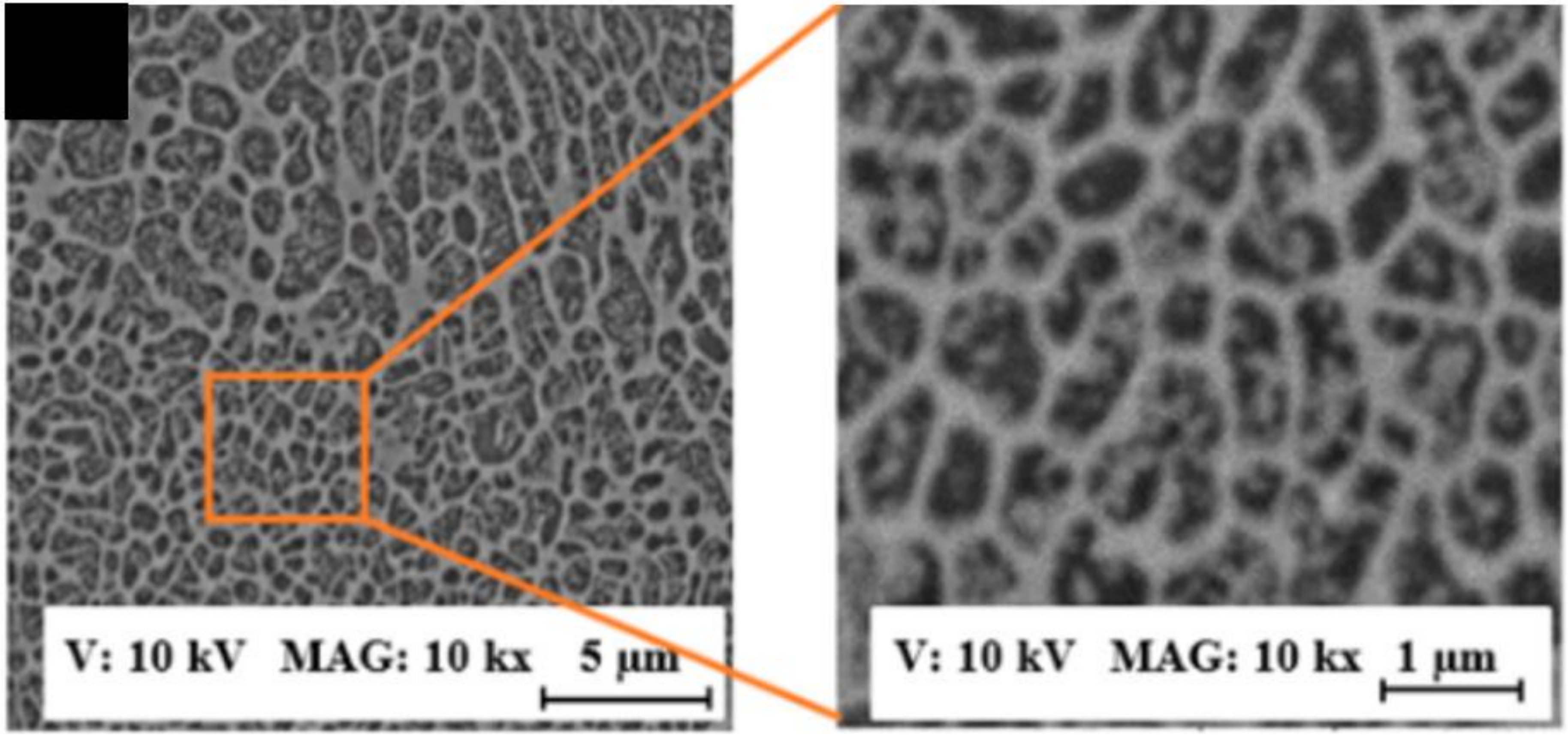

Fig. SEM micrographs showing submicron cellular structures in AMed as-built AlSi10Mg

Source: Maamoun et al. 2018 [https://doi.org/10.3390/ma12010012]

AlSi10Mg

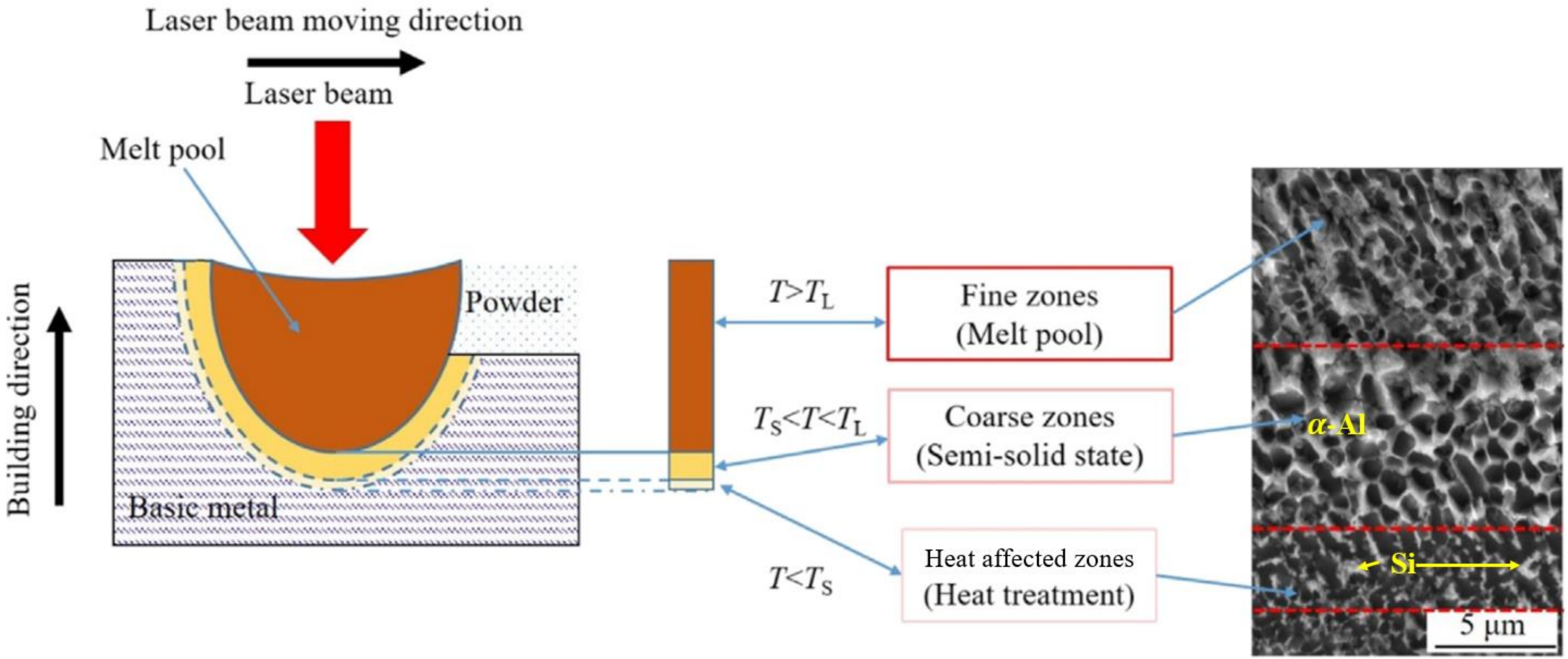

Fig. Schematic representation of the creation of the three zones observed in LPBFed AlSi10Mg (T_L and T_S are the liquidus and solidus temperatures, respectively)

Source: Maamoun et al. 2018 [https://doi.org/10.3390/ma12010012]

AlSi10Mg

Fig. Comparing mechanical properties AlSi10Mg specimens optimised through machine learning (shown as yellow stars) to the UTS and elongation of LPBFed AlSi10Mg in other publications

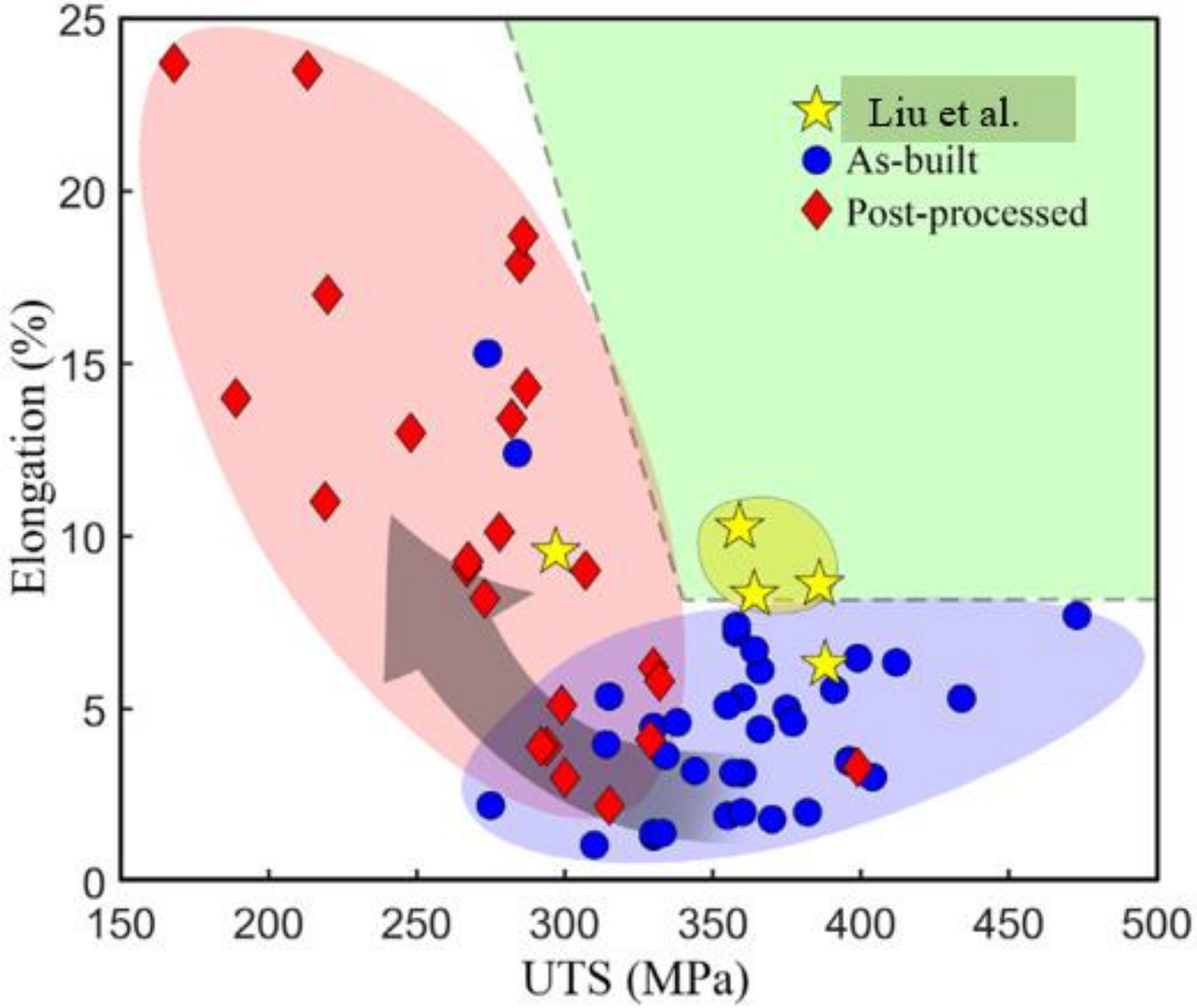

Source: Liu et al. 2020 [https://doi.org/10.1016/j.actamat.2020.10.010]

AlSi10Mg

Fig. Engineering stress–strain curves of AlSi10Mg samples in the LPBF as-built (AB), LPBF and direct aged (DA), LPBF and stress relieved (SR), preheated (PH) LPBFed, and Ascast and T6 (AC T6) conditions, as listed in Table 8.2. Samples were printed in horizontal (XY) and vertical (Z) building orientations with respect to the substrate

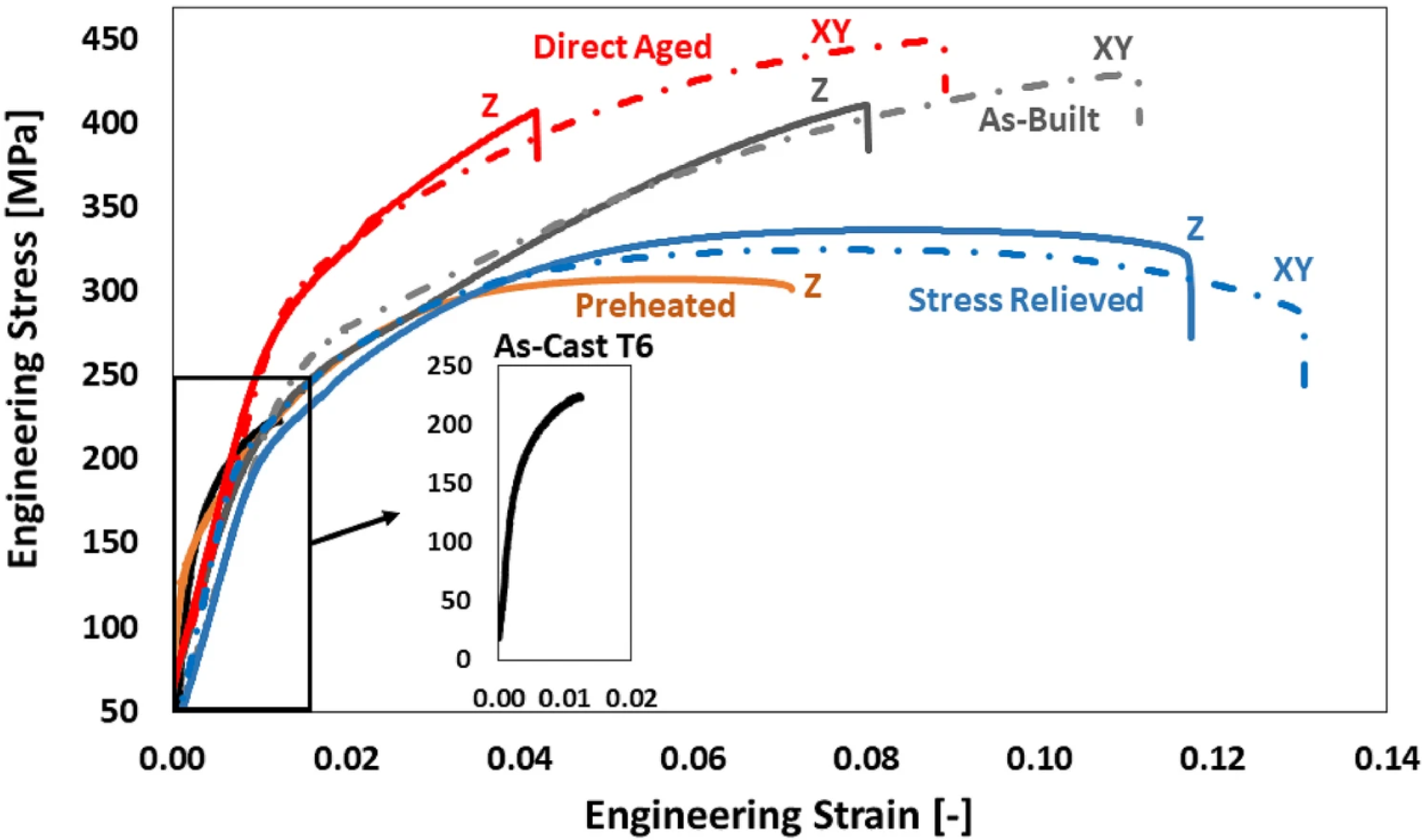

Source: Cauwenbergh et al. 2021 [https://doi.org/10.1038/s41598-021-85047-2]

AlSi10Mg

Fig. Fracture surfaces of LPBFed AlSi10Mg showing (a) lack of fusion (LOF) defects, (b) various regions of crack initiation, (c) ridges, (d) fatigue striations, and (e) parabolic striations

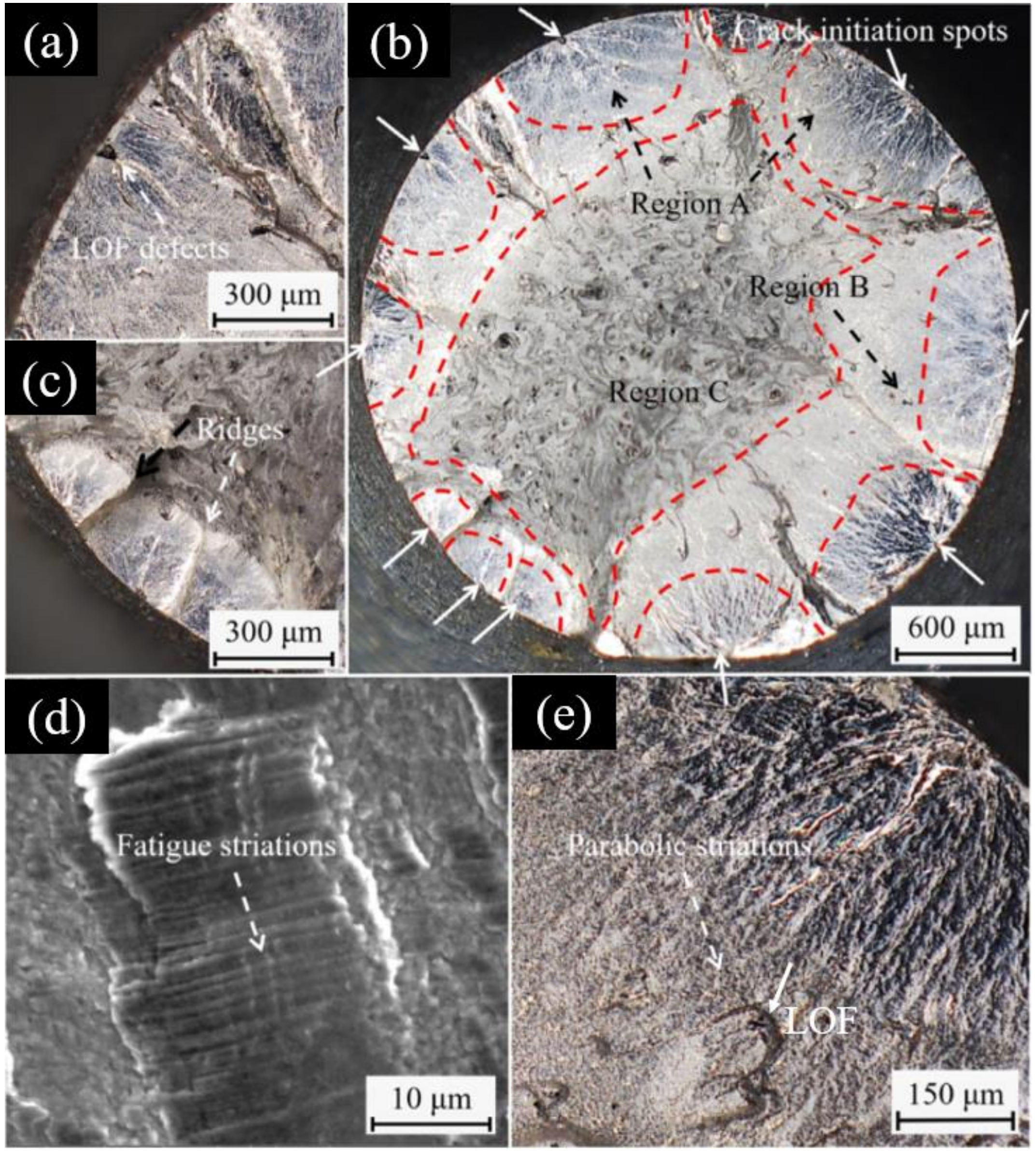

AlSi10Mg

Fig. Fracture surfaces of LPBFed AlSi10Mg showing non melted particles in (a) and (c), LOF defects in (b) and (d), melt pool boundaries in (d), and dimples in (e)

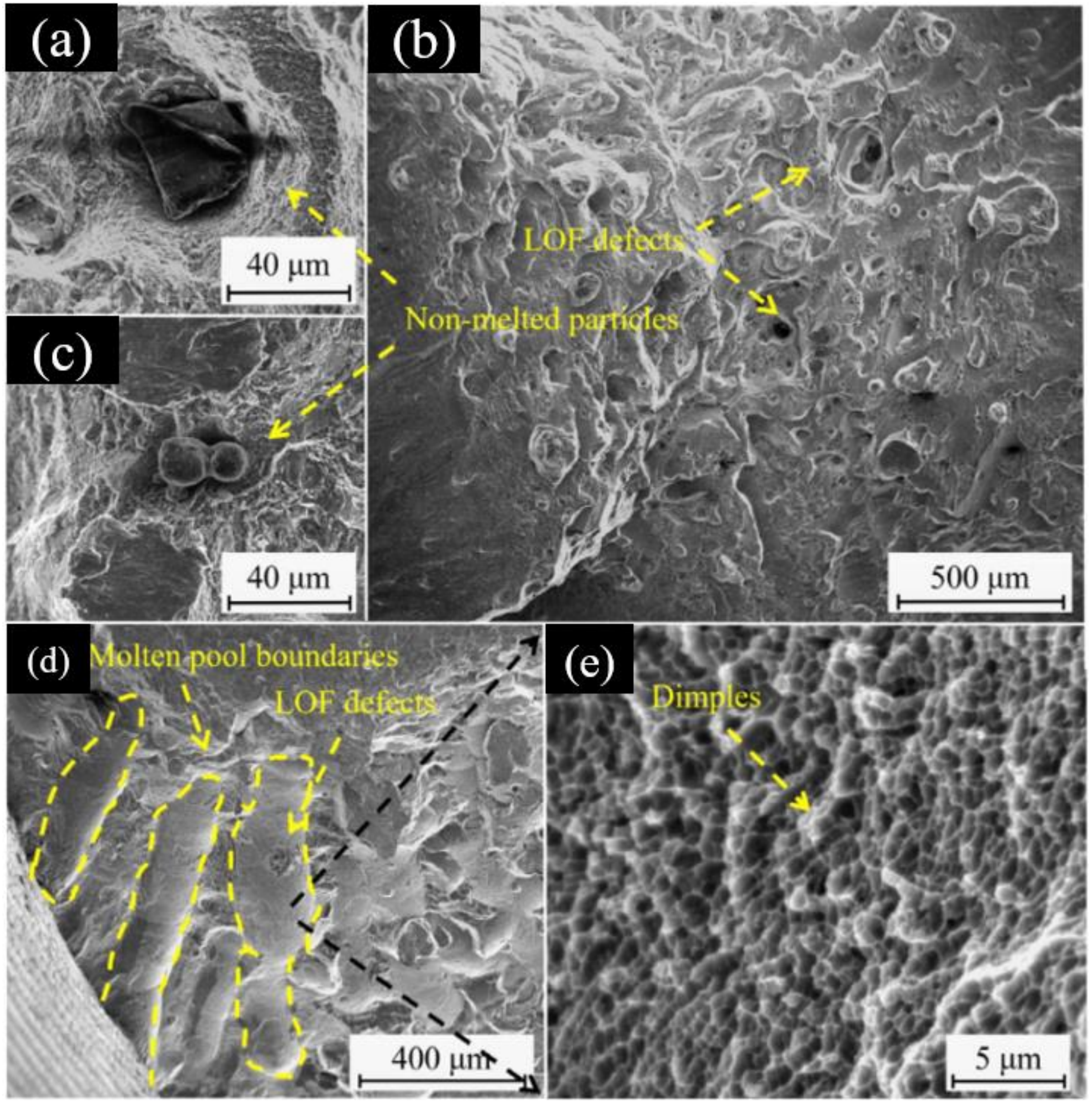

Source: Liu et al. 2020 [https://doi.org/10.1016/j.actamat.2020.10.010]

AlSi12

Fig. SEM micrograph of the LPBFed as-built AlSi12 along (a) scan direction and (b) building direction (the insets in a and b show the high magnification areas in the white rectangles, showing Si particles), (c) Typical tensile stress-strain curves of the LPBFed as-built AlSi12, (d) Tensile properties of the LPBFed as-built AlSi12 (shown by a star) compared to those of the reference LPBFed as-built AlSi12 and AlSi10Mg alloys reporting different studies from literature (MP: melt pool)

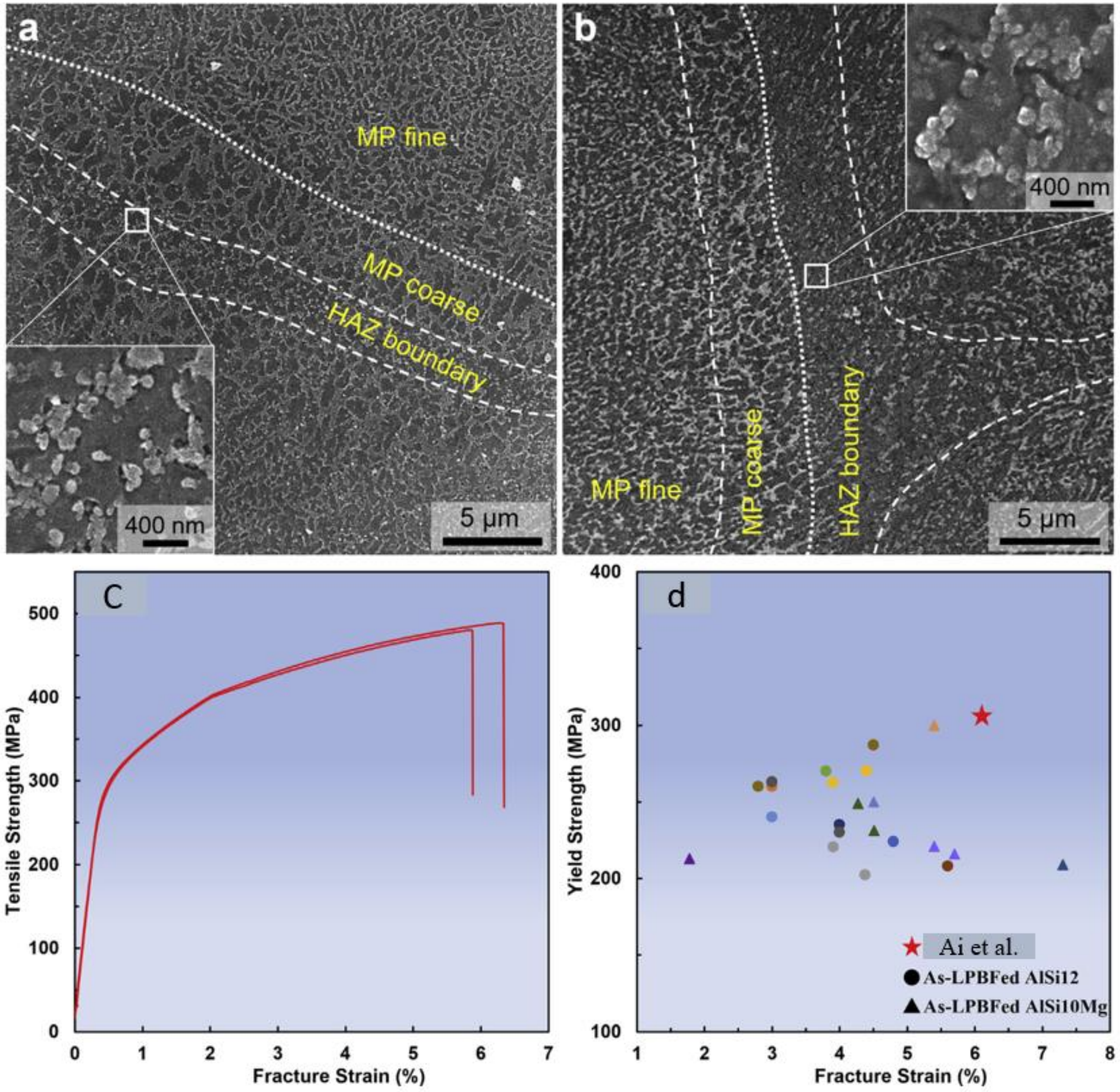

Source: Ai et al. 2022 [https://doi.org/10.1016/j.jmrt.2022.04.008]

AlSi12

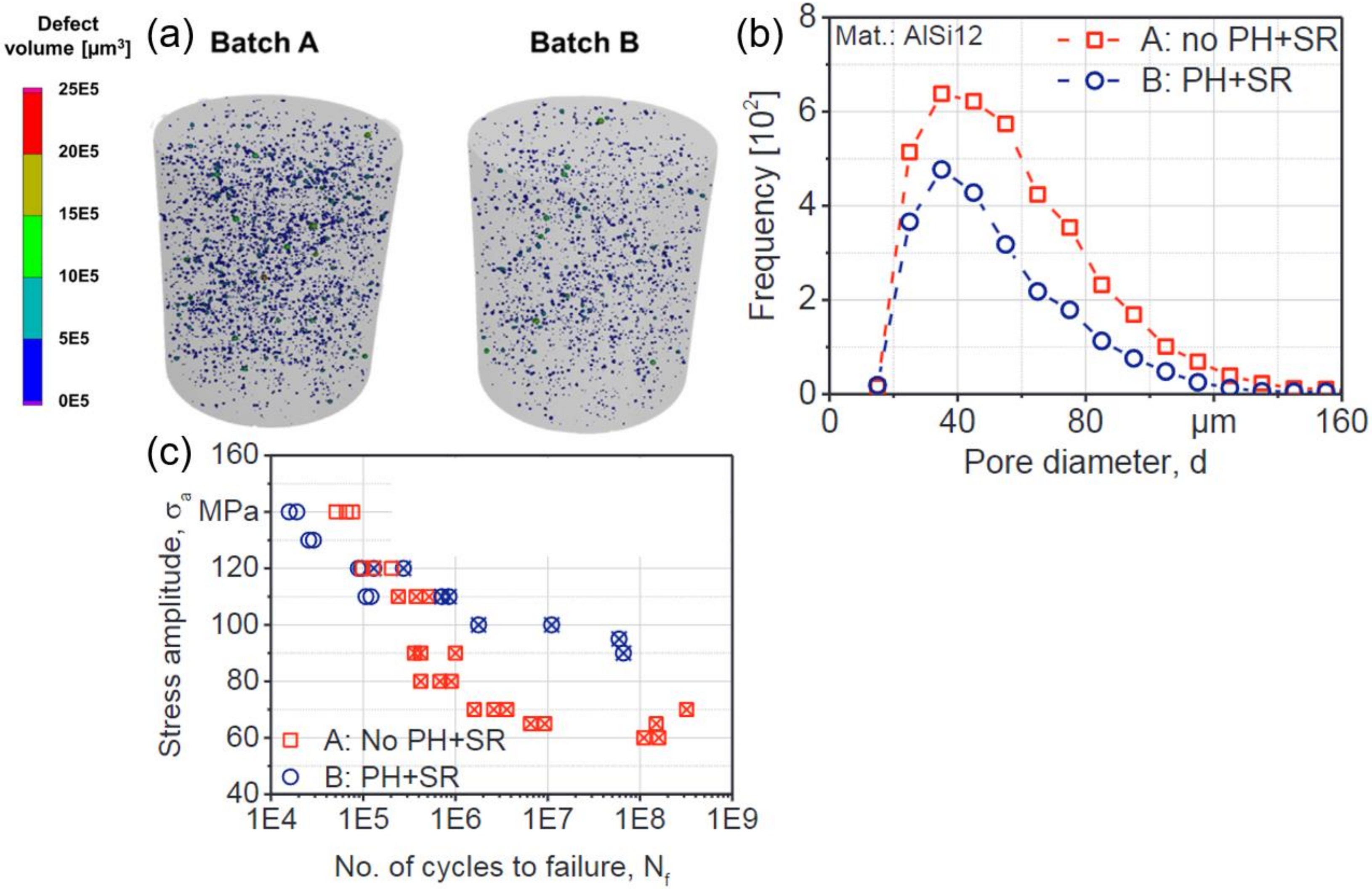

Fig. (a) 3D representation of the pores in the LPBFed AlSi12 after various heat treatments taken by X-ray tomography, (b) Number and size of pores in LPBFed AlSi12 after various heat treatments, (c) High cycle fatigue of LPBFed AlSi12 after various heat treatments showing better fatigue properties of batch A at the beginning and superior properties of batch B at the end of high cycle fatigue

Source: Awd et al. 2020 [https://doi.org/10.1016/j.tafmec.2020.102483]

AlSi12

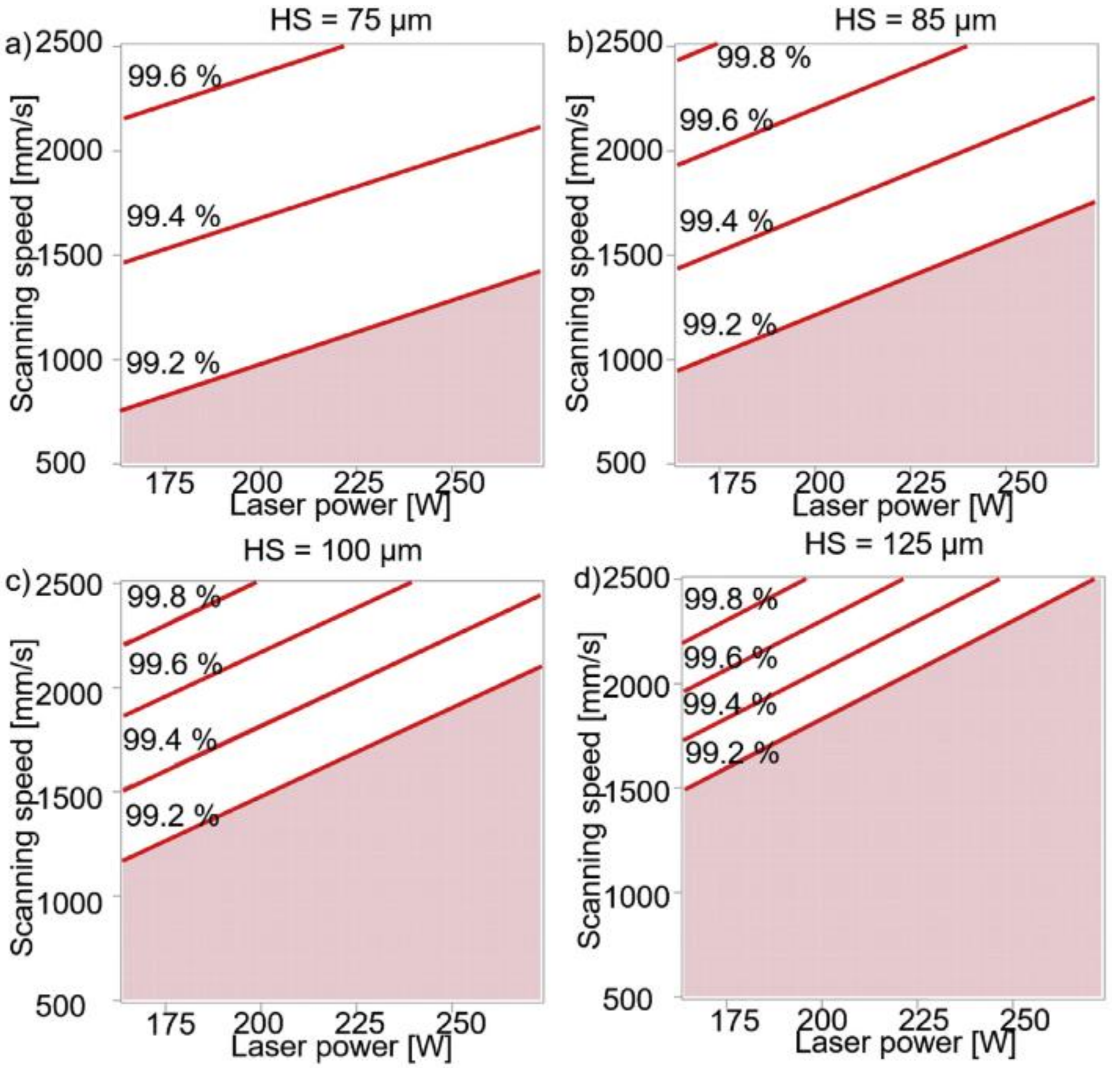

Fig. Densities of the LPBFed AlSi12 samples produced with variations of P and v, and (a)-(d) HS = 75 µm, HS = 85 µm, HS = 100 µm, and HS = 125 µm, respectively

Relative density using ANOVA analysis:

$$\rho(\%) = 100.2 - 0.004P + 0.0005v - 0.01HS - 0.0001(P - 225.6)(HS - 92.2) + 0.00002(v - 1591)(HS - 92.2).$$

Where,
ρ: relative density
P: laser power in W
v: scan speed in mm/s
HS: hatch spacing in µm

(The LPBF parameters that result in a density less than 99.2% are present in the red area. Isoresponses, or lines of constant density, are shown in red)

Source: Gheysena et al. 2021 [https://doi.org/10.1016/j.matdes.2020.109433]

Scalmalloy

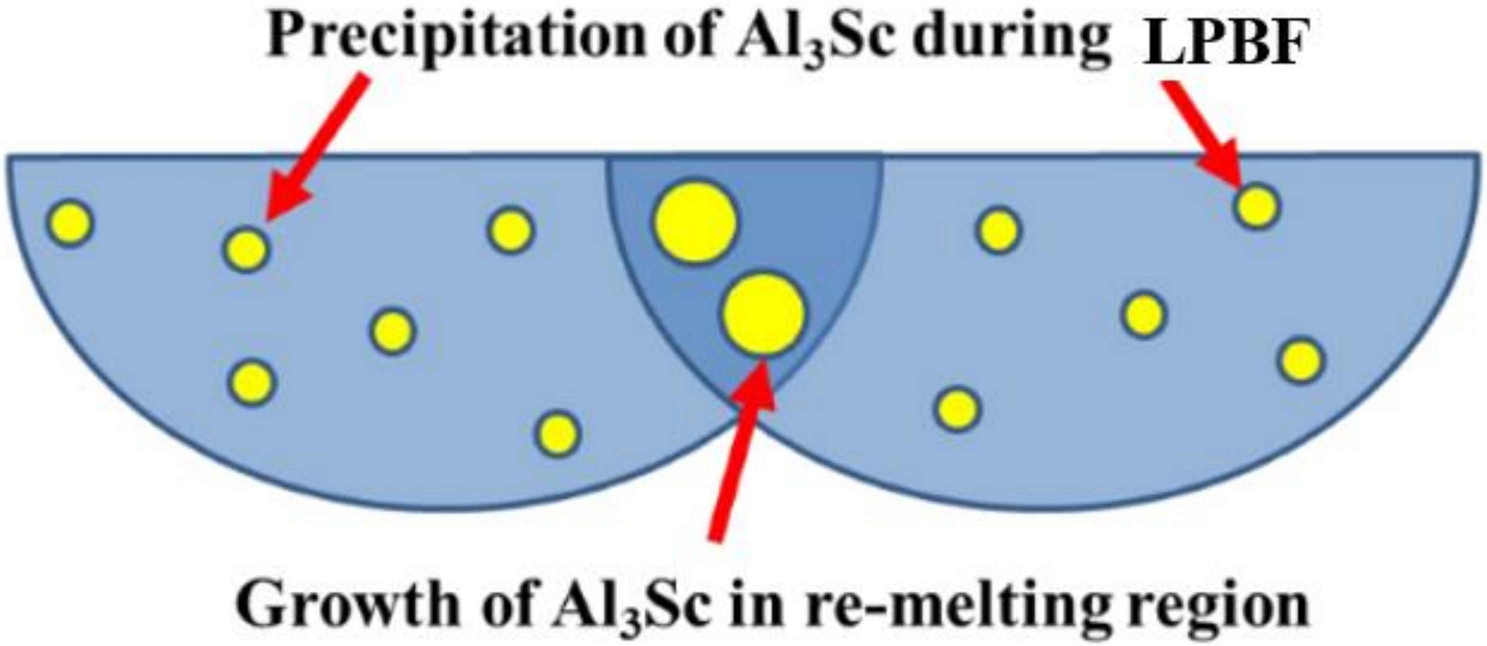

Fig. Schematic representation of the precipitate size variation brought on by various melt pool heat histories during AM of Scalmalloy

Source: Kuo et al. 2021 [https://doi.org/10.3390/met11040555]

Scalmalloy

Fig. (a) Optical and (b) SEM micrograph showing the typical microstructure of the LPBFed as-built Scalmalloy
(CG and EG are columnar and equiaxed grains, respectively, and the build direction is shown with the yellow arrow)

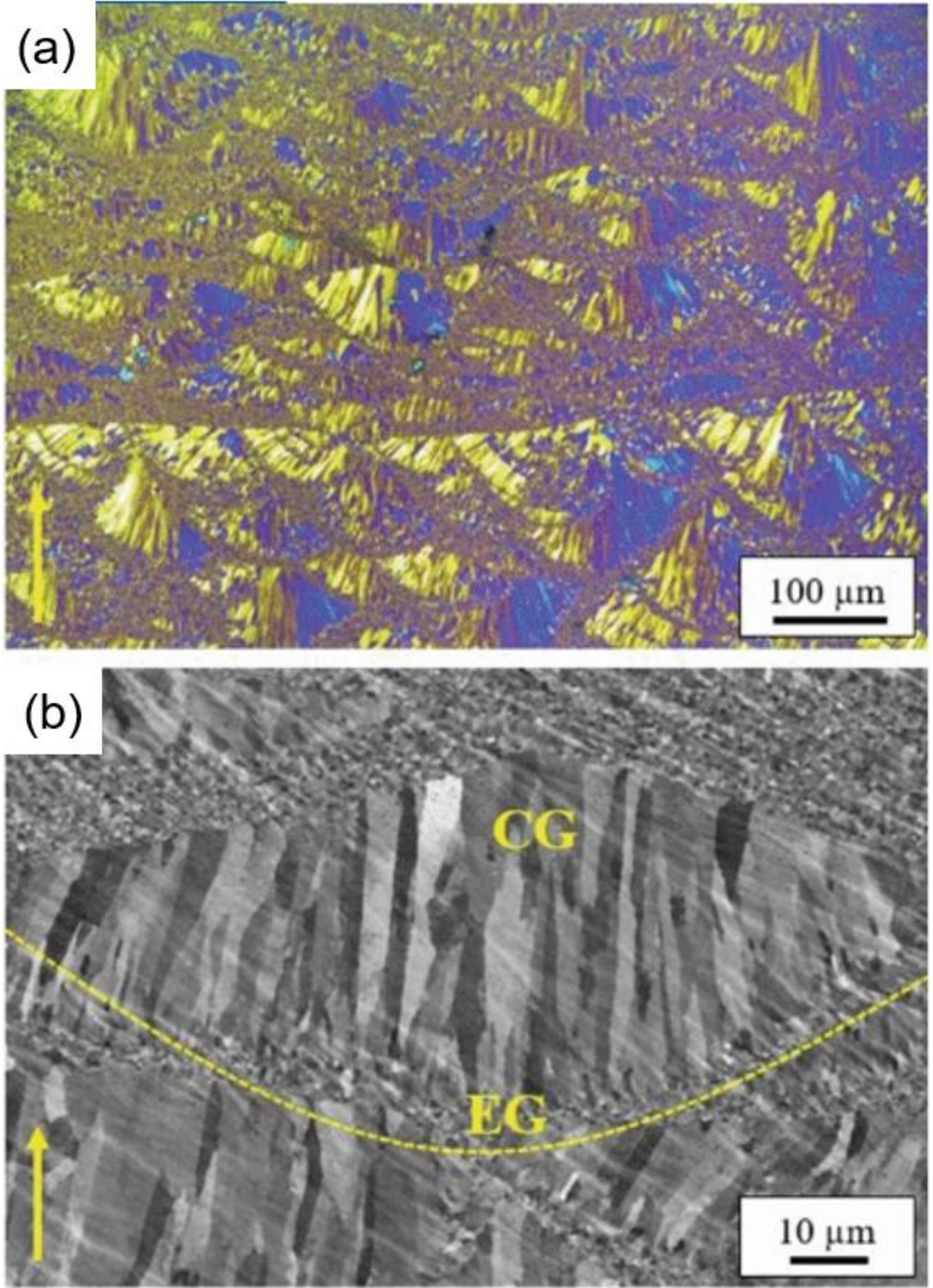

Source: Bartl et al. 2022 [https://doi.org/10.1007/s11665-022-06592-z]

Scalmalloy

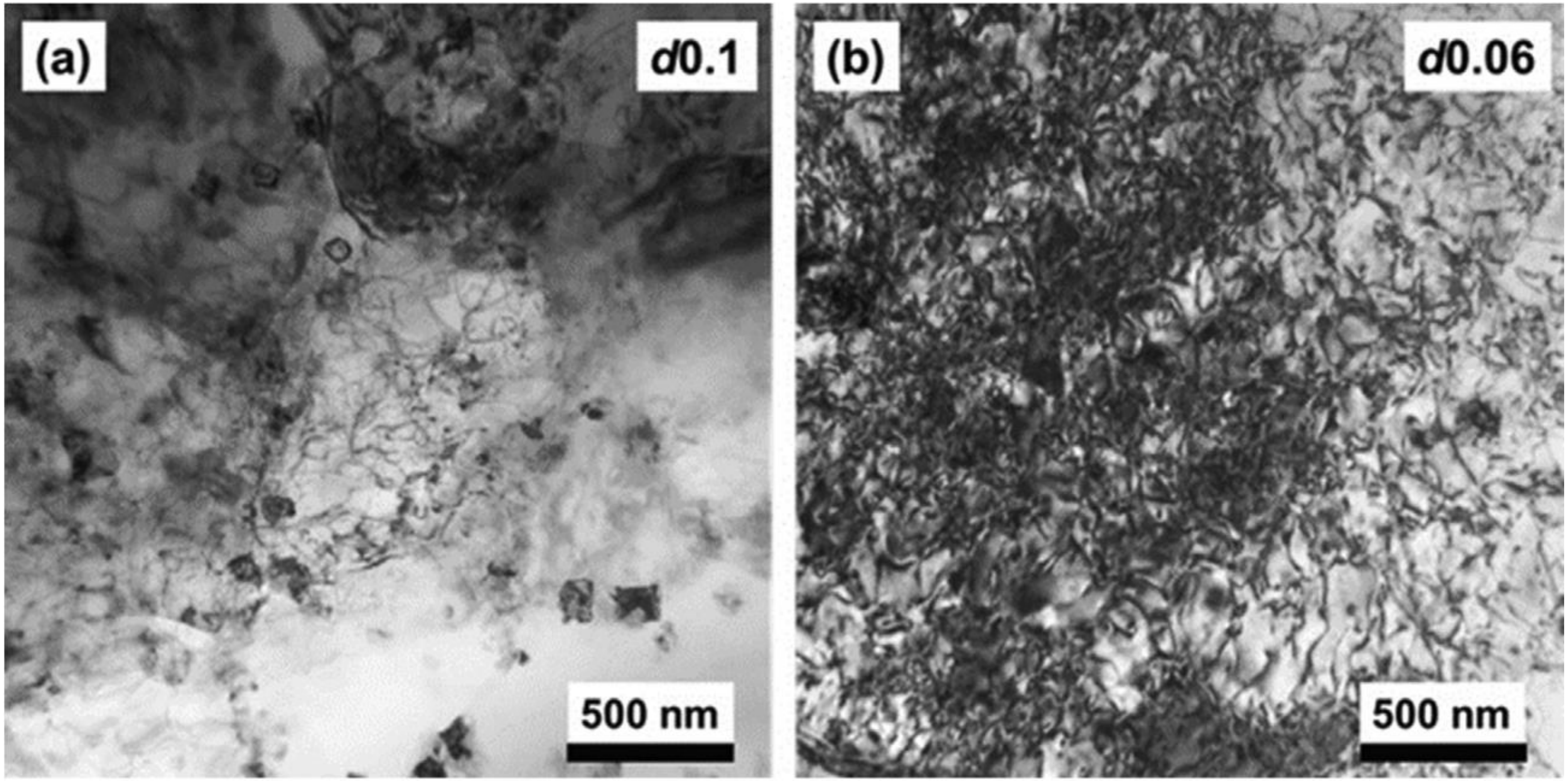

Fig. Dislocation structure of the FG regions of two LPBFed as-built Scalmalloy built with (a) hatch distance of 100 µm (d0.1) and (b) hatch distance of 60 µm (d0.06)

Source: Ekubaru et al. 2022 [https://doi.org/10.1016/j.matdes.2022.110976]

Scalmalloy

Fig. (a) - (g) HAADF-TEM micrographs in a FG region of a LPBFed Scalmalloy showing the presence of various precipitates, (h) Bright field TEM micrographs showing grain boundary pinning of a columnar grain, indicated by arrows, (i) a fine grain, and (j) magnification of a grain boundary in a fine grain. The selected area diffraction pattern shows presence Al_3Sc at the grain boundaries

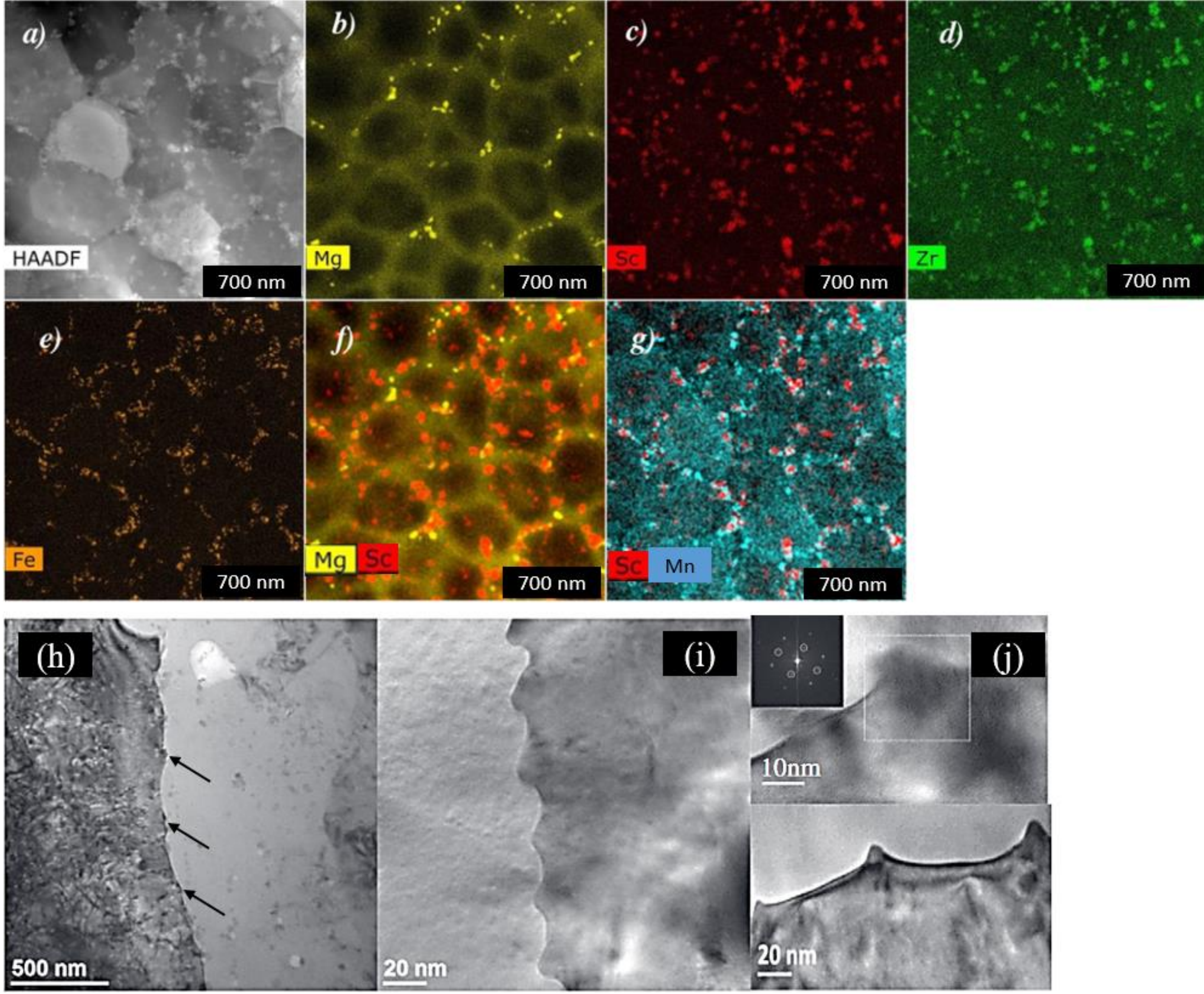

Source: Spierings et al. 2017 [https://doi.org/10.1016/j.matdes.2016.11.040]

Scalmalloy

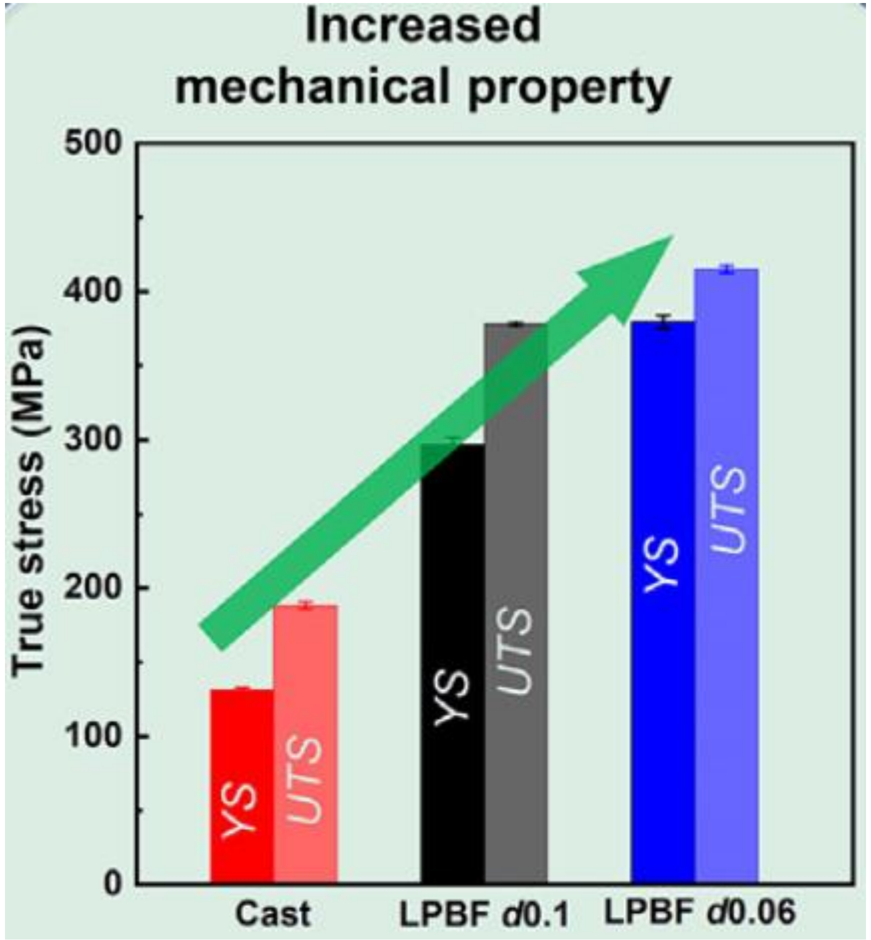

Fig. Comparison between the yield strength (YS) and ultimate tensile strength of two LPBFed Scalmalloy samples produced with the same processing parameters, but different hatch spacings of 100 µm (d0.1) and 60 µm (d0.06), and their cast counterpart

Source: Ekubaru et al. 2022 [https://doi.org/10.1016/j.matdes.2022.110976]

Scalmalloy

Fig. EBSD micrographs of the x-z plane of LPBFed Scalmalloy after dynamic loading, showing the crack tip area for the following orientations: (a) horizontal, (b) diagonal, (c) vertical, and (d) flat build. (e) Apparent crack growth resistance curves for edge-notched three-point bend specimens under dynamic loading conditions. It is worth noting that the coordinates shown on the component's schematics are separate from the coordinates shown on the EBSD micrographs

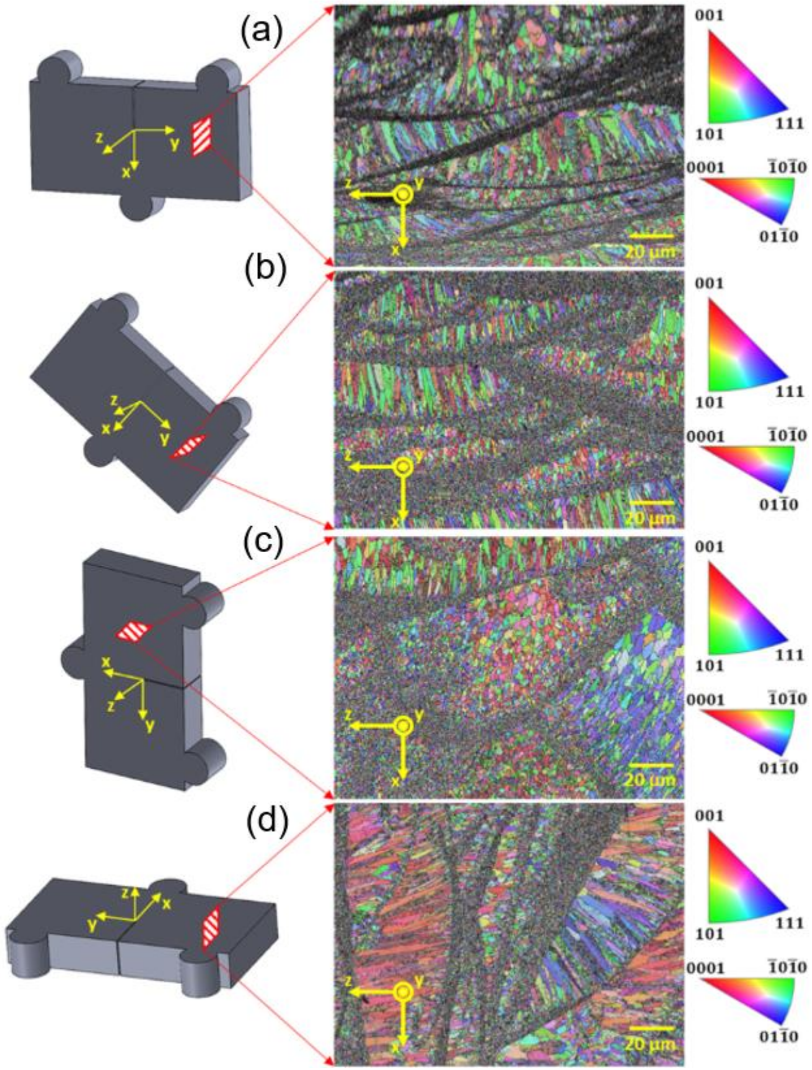

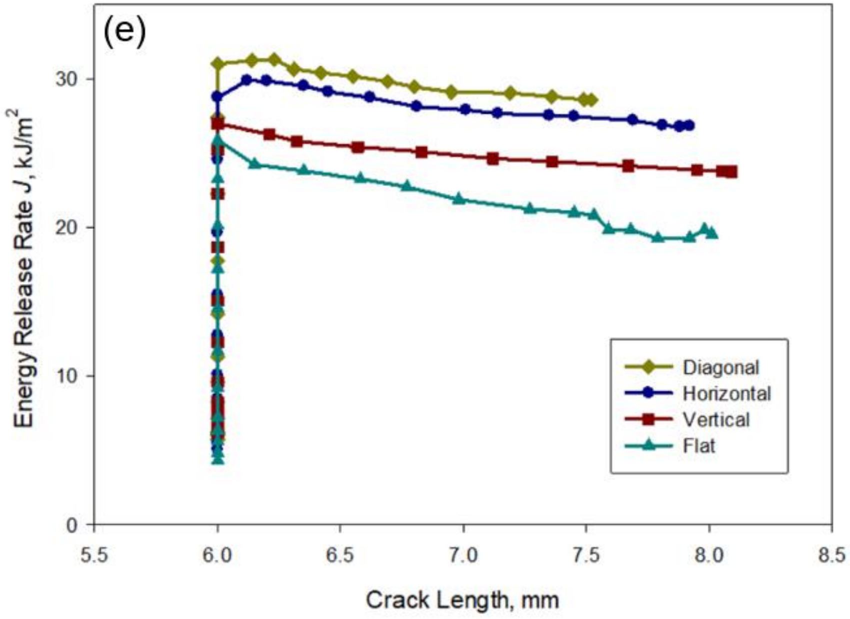

Source: Isaac et al. 2021 [https://doi.org/10.1016/j.msea.2021.141978]

AlSi7Mg(A357)

Fig. LPBFed A357 TEM micrographs displaying the solidification Al cells in the (a) LPBFed as-built and (b) SHTed for 1 h samples, (c) XRD patterns displaying the peaks of the eutectic Al and Si phases, and (d) the silicon content in the matrix under various conditions

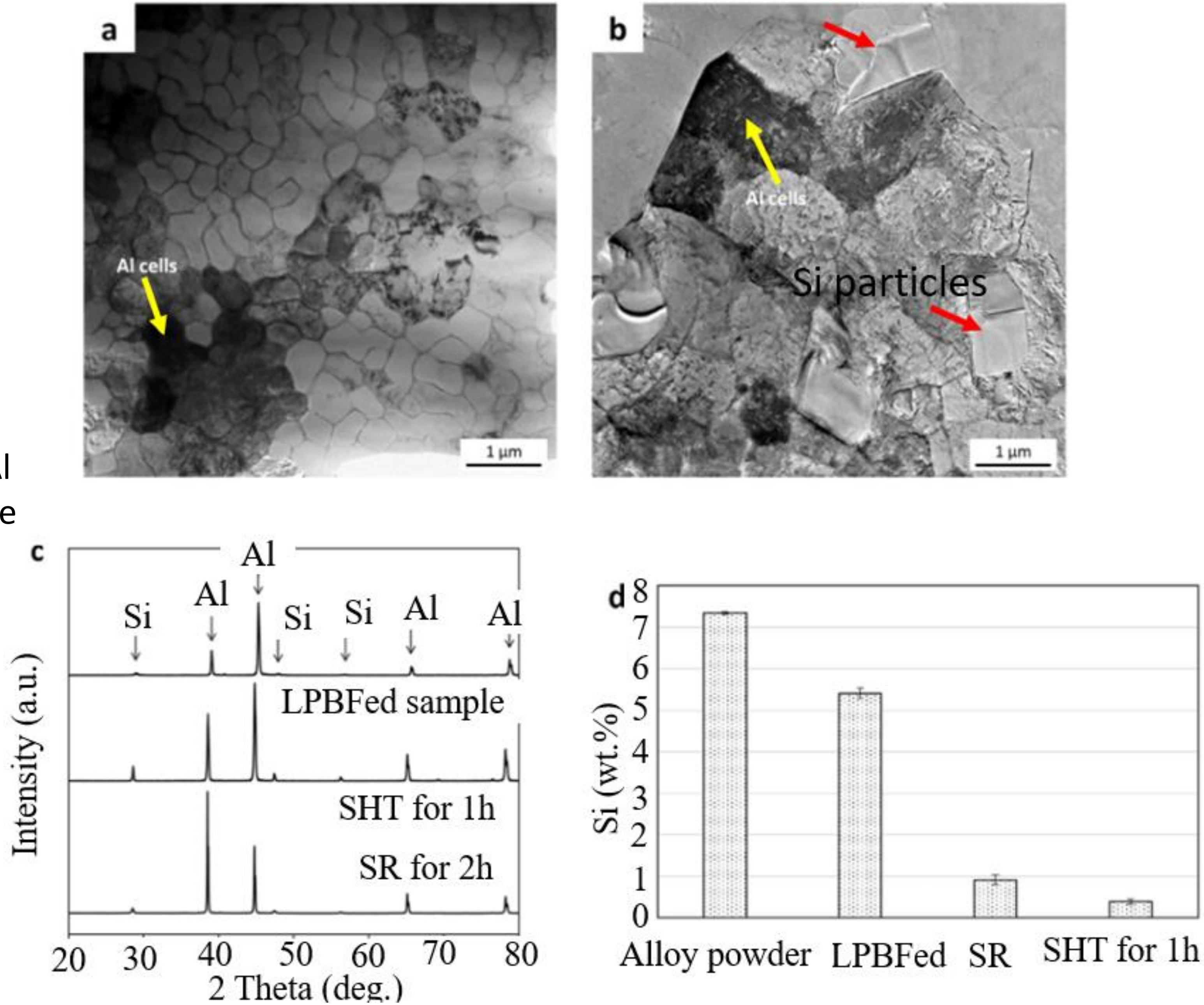

Source: Rao et al. 2017 [https://doi.org/10.1016/j.addma.2017.08.007]

AlSi7Mg(A357)

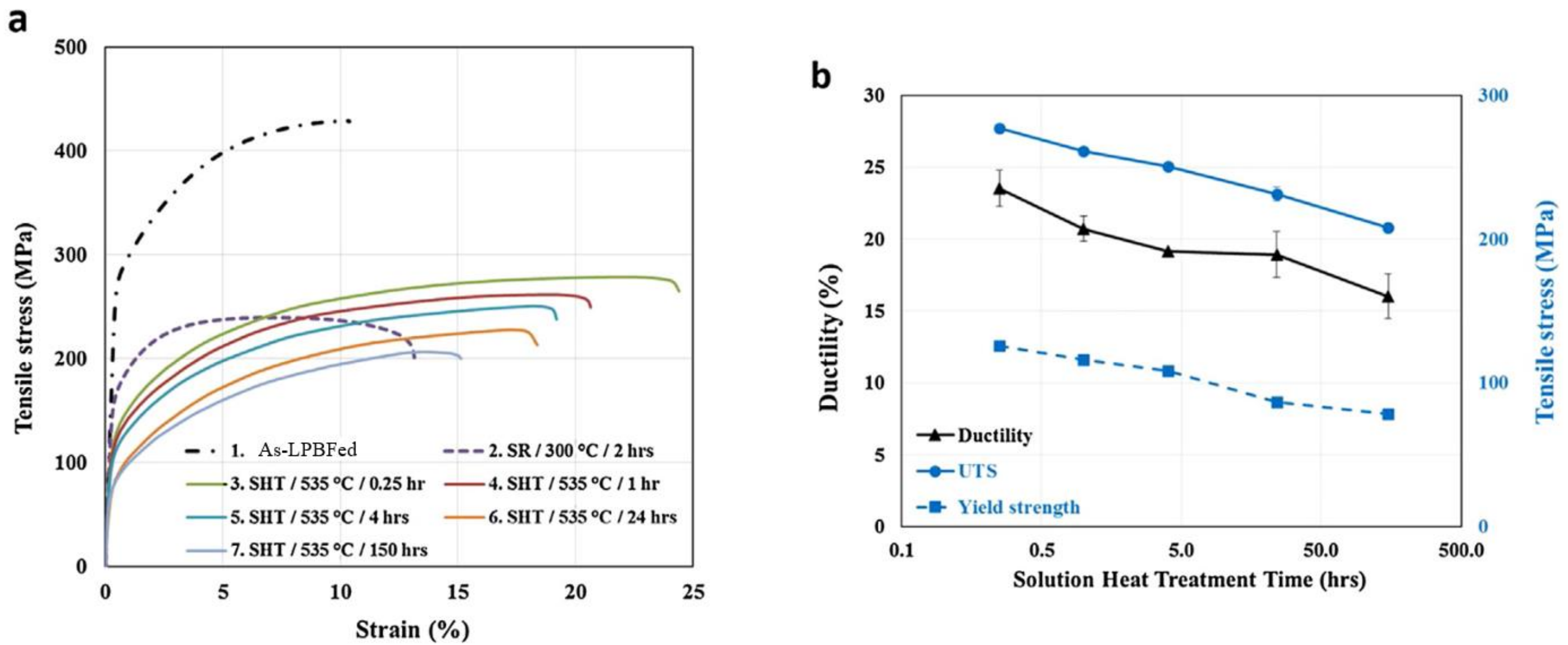

Fig. (a) Engineering stress-strain curves of LPBFed samples under as-built and various heat-treated conditions. (b) The tensile properties of LPBFed A357 alloy samples SHTed over various durations

Source: Rao et al. 2017 [https://doi.org/10.1016/j.addma.2017.08.007]

AlSi7Mg(A357)

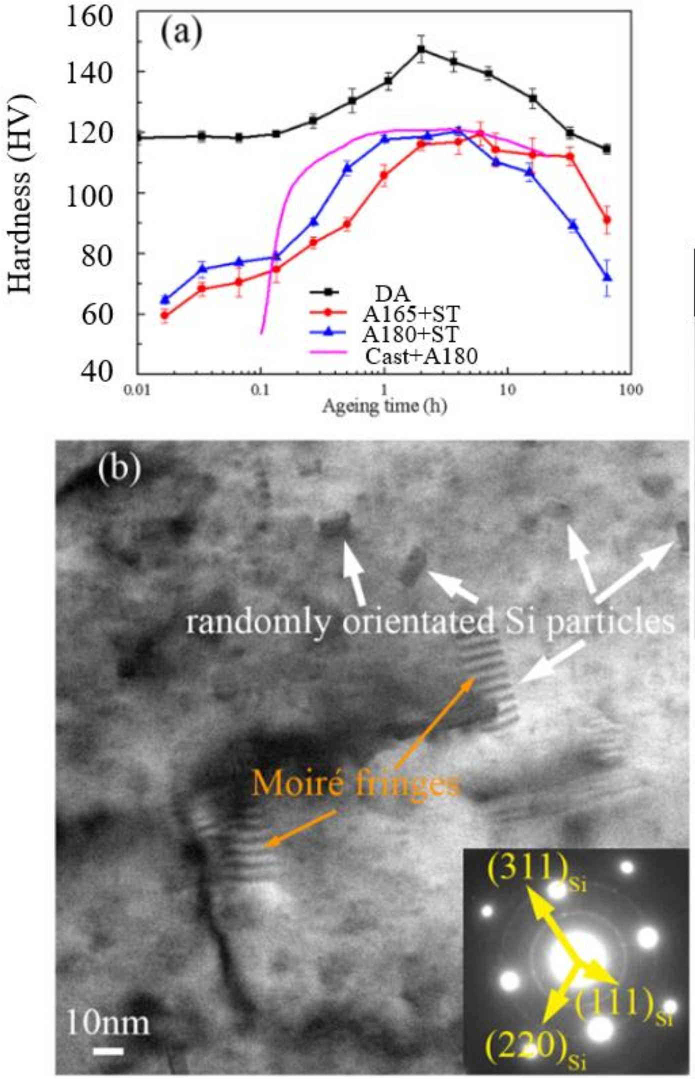

Fig. (a) Hardness curves for LPBFed A357 alloy and cast A357 after various heat treatment schemes, including direct ageing (DA) at 165◦C, solution treatment at 535◦C for 1 h followed by ageing at 165◦C (A165+ST), solution treatment at 535◦C for 1 h followed by ageing at 180◦C (A180+ST), and as-cast sample after ageing at 180◦C (cast+A180), (b) TEM micrograph of LPBFed A357 alloy with randomly oriented Si particles aged for two hours (peakaged condition).

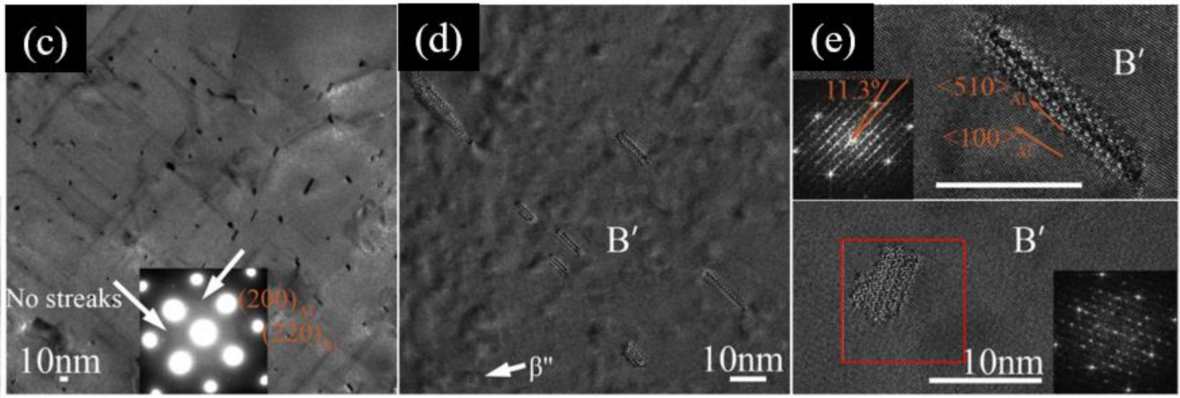

Fig. (c) TEM micrograph showing the Al matrix filled with precipitates of B′ and β′′ shown in (d) and (e) after 1 hour of solution treatment, followed by 6 hours of ageing

Source: Rao et al. 2019 [https://doi.org/10.1016/j.scriptamat.2018.09.045]

AA6061

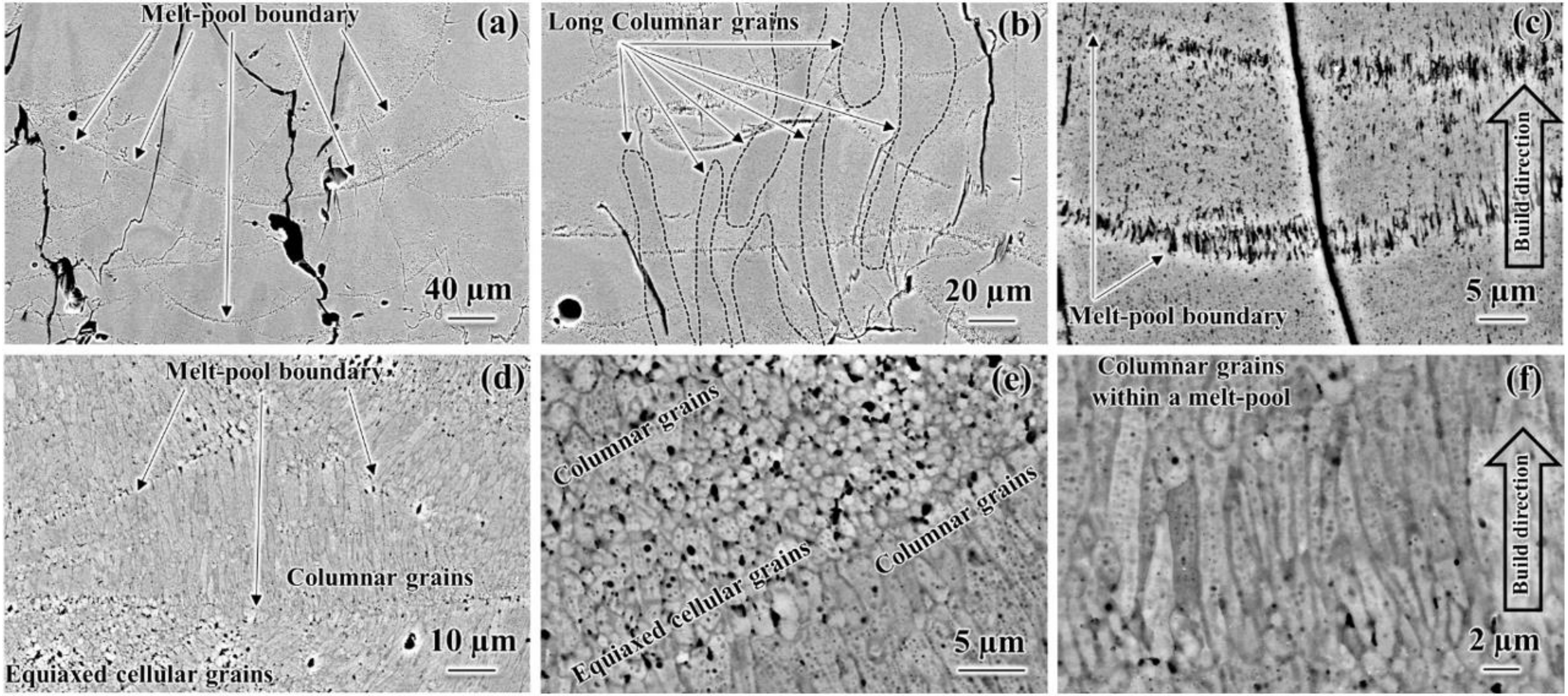

Fig. SEM micrographs taken from the cross-sections of the (a)-(c) original and (d)-(f) Zr-modified AA6061 alloys in their LPBFed as-built states

Source: Mehta et al. 2021 [https://doi.org/10.1016/j.addma.2021.101966]

AA6061

Fig. Schematics of crack formation in original AA6061 and crack prevention in Zrmodified AA6061 fabricated with LPBF

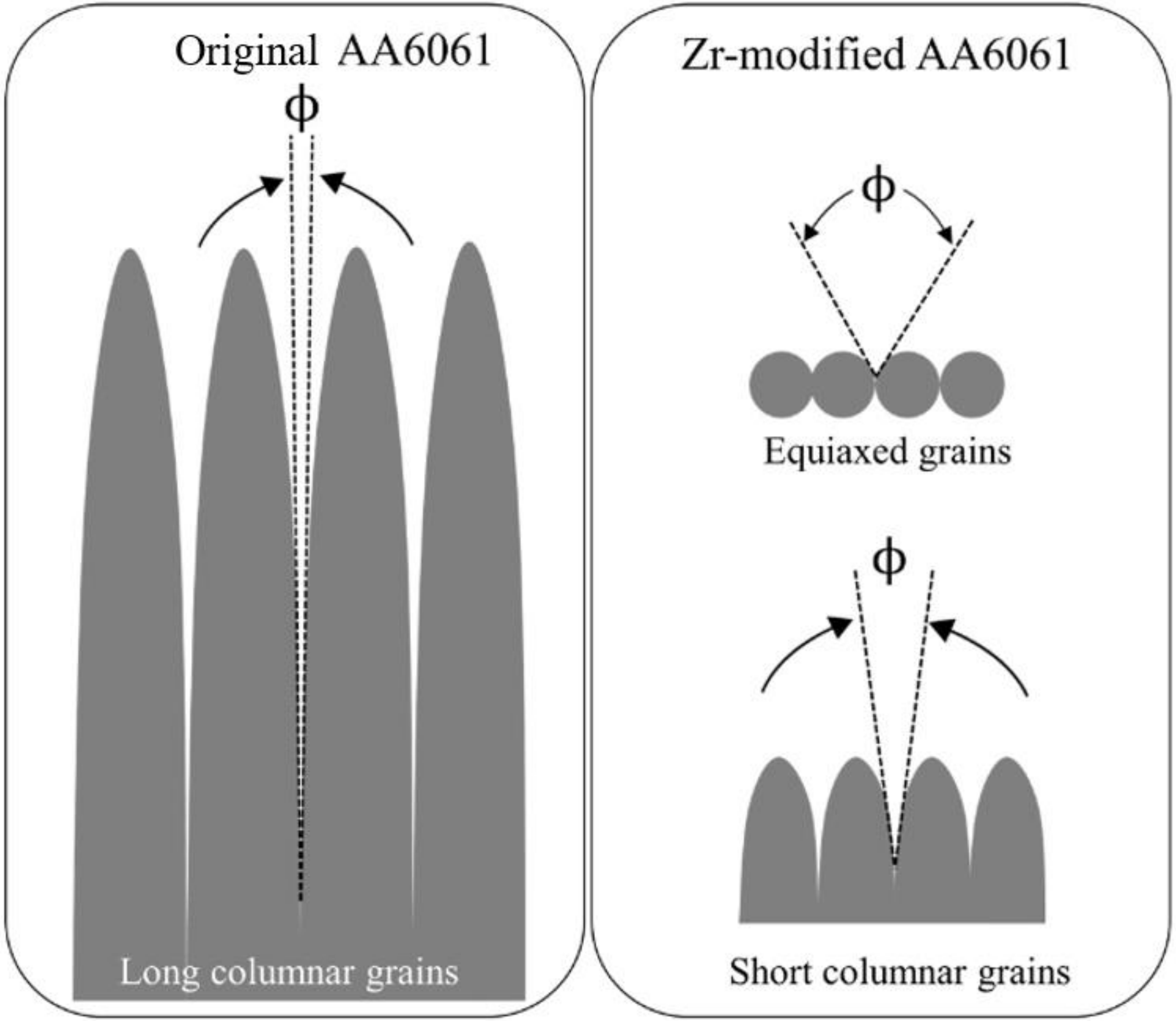

Source: Mehta et al. 2021 [https://doi.org/10.1016/j.addma.2021.101966]